Near-surface geophysical investigation of a gravel site near Whitehorse, Yukon

Y.K. Lee[1], C.-G. Bank*
Department of Earth Sciences, University of Toronto
[1]now with PETRONAS, Kuala Lumpur, Malaysia

S. Laxton
Yukon Geological Survey

Lee, Y.K., Bank, C.-G. and Laxton, S., 2017. Near-surface geophysical investigation of a gravel site near Whitehorse, Yukon. *In:* Yukon Exploration and Geology 2016, K.E. MacFarlane and L.H. Weston (eds.), Yukon Geological Survey, p. 141-148.

ABSTRACT

Three near-surface geophysical survey methods - electrical resistivity tomography (ERT), ground-penetrating radar (GPR), and seismic refraction tomography - were used along a 96 m transect to compare the suitability of these techniques in determining the thickness of a gravel layer. ERT shows three distinct layers: a high resistivity layer (~4000 Ωm) at depth 2-8 m, sandwiched between low resistivities (~2000 Ωm). GPR results show two prominent subhorizontal reflections, one around 1 m and a second around 6 m depth with dipping reflections in between. Seismic refraction data show sharp velocity changes and seismic refraction tomography images a similar layering. We tentatively interpret the top layer in all three methods (above ~2 m) as soil, the middle layer (to ~8 m) as gravel, with glacial till below. Each method is useful to imaging the gravel, though we prefer ERT because it provides quick results that are straight-forward to interpret.

* *charly.bank@utoronto.ca*

INTRODUCTION

The application of near-surface geophysical techniques is useful in determining the thickness of aggregate deposits, which have the potential for high commercial value. Gravel deposits result from the weathering and erosion of rocks and can provide aggregate for constructing roadways and buildings. In cooperation with the Yukon Geological Survey, we explored a potential aggregate quarry in Whitehorse, Yukon. The region is rich in glacial till and gravel, as evident from existing aggregate quarries in the area. Bond (2004) mentions that the till and gravel found within this area were likely deposited during the McConnell Glaciation, which covered the area under 1.3 km of ice, and started retreating ~13,000 years ago. The ensuing glacial meltwater formed glacial lakes Champagne and Laberge, which covered the Whitehorse valley. The glacial meltwater deposited glaciofluvial gravel and glaciolacustrine deposits consisting of sand, silt and clay. Ultimately, the glacial lake drained, leaving behind most of the fine-grained sediment in the Whitehorse region (Bond, 2004). The areal extent of the gravel site is evident upon examination of aerial photographs of the area, but the thickness of the gravel layer has yet to be determined. Hence our team conducted a survey at this gravel site.

Laxton and Coates (2015) conducted ground penetrating radar (GPR), induced polarization tomography and electrical resistivity tomography (ERT) surveys at four sites in the vicinity of Whitehorse with the objective of estimating the quantity and quality of potential aggregate resources. One of their survey sites was near McLean Lake, which is ~2 km away from our site. Their results show the presence of a thin gravel and boulder deposit 5 to 10 m thick. They also estimated that fifty thousand cubic metres of gravel are likely located in this deposit; however, a large quantity of boulder material would complicate excavation and processing of the aggregate.

Our survey has two main objectives: 1) to determine the thickness of the gravel layer, and 2) to evaluate the suitability of three different methods for achieving this. The three methods are: ERT, seismic refraction tomography and GPR.

STUDY SITE

Field investigations were undertaken in Whitehorse, Yukon, one kilometre southwest of McLean Lake Road on the west side of the Copper Haul Road. The site lies 5.5 km southwest of the Whitehorse airport, and about 2 km away from an existing aggregate quarry. The geophysical investigations were run along a 96 m transect (UTM zone 8V, WGS84 datum, start: 494549E, 6724066N; end: 494531E, 6724159N). Figure 1, an airphoto of the site, reveals the different types of vegetation growing on the gravel outwash.

METHODS

During mid-June 2015, our team of eight undergraduate students and one faculty member carried out near-surface geophysical surveys on the site. Three geophysical methods were used along the same 96 m long profile which extends from the edge of the deposit towards its centre in an east-west direction.

ELECTRICAL RESISTIVITY TOMOGRAPHY

ERT is commonly used to define the ground water table, subsurface layers and depth of bedrock. We inserted 48 electrodes into the ground and connected them to an IRIS Syscal Junior switch-48 multi-electrode resistivity core (Fig. 2a). The core sends electric current via two electrodes into the ground and the voltage is measured between another two electrodes. Resistivity values are then calculated and the nature of the layers inferred. The resistivity of rock and sediment is dependent on several factors, including: water saturation, porosity, pore fluid chemistry, mineral composition and stratification of the host rock or sediment material (Lucius *et al.*, 2008). For a deeper signal penetration, larger electrode spacing is used. We chose the Wenner array because it has a high signal strength and affords good vertical resolution (Loke, 2016).

In our survey, the 48 electrodes were placed at 2 m intervals along the 96 m profile starting at 0 m. The Wenner array selects four equally spaced electrodes where the outer two electrodes are the current electrodes, and the inner two electrodes are the potential electrodes. The array spacing expands about the array midpoint which moves along the line to measure a profile (Sharma, 1997). The data are inverted using the res2Dinv software to produce a resistivity section which best explains the data (Geotomo, 2009). Figure 2b shows the measured profile (called pseudosection) at the top, the result of the inversion on the bottom, and the calculated data in the center. The inversion will proceed until this calculated data profile closely matches the observed one. The software assumes a two-dimensional subsurface resistivity structure and smooth contrasts - as opposed to sudden changes - to remain numerically stable.

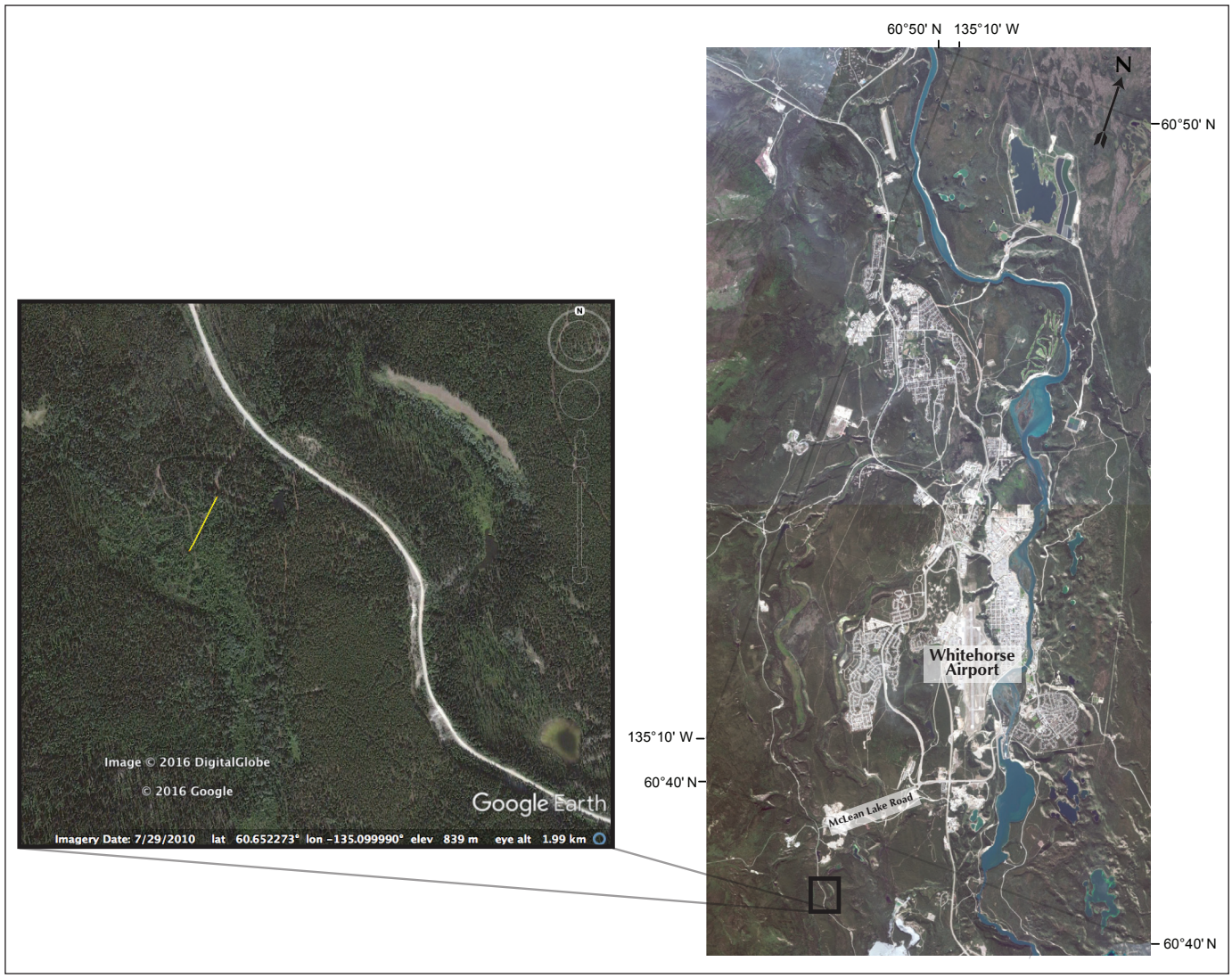

Figure 1. *Google Earth image of the site. The yellow line marks the approximate location of our 96 m long survey line. The surface extent of the gravel is marked by the different vegetation (lighter coloured poplar surrounded by darker coloured pine trees).*

GROUND PENETRATING RADAR

GPR works by transmitting radio waves into the ground via an antenna and recording the reflected signals with a receiver. A contrast in dielectric values of the subsurface will cause reflections, and the equipment records the two-way travel time of the waves returning to the surface. The time from transmitting to receiving depends on both the dielectric constant (which determines how fast the radar wave propagates in the ground) and the depth to the reflector. Hence by having the arrival times of each spot, we can deduce the depth to the reflector only if we know the radar velocity. This method is more intuitive to use in the field compared to the other two methods mentioned above because real-time results are visible on the control panel console screen during the survey.

To collect GPR data, we pulled the GSSI SIR-3000 unit connected to a100 MHz, 200 MHz or 400 MHz antenna along the ground surface to avoid free air reflections (Fig. 3a). A calibrated survey wheel, attached to the antenna, measured the distance travelled. The data were viewed using MATLAB software. The sample radargram sections in Figure 3b were collected with the different antenne along the same short profile. All three show similar features, for example a strong undulating reflector above 20 ns and a subhorizontal reflection around 120 ns. We found the 100 MHz antenna to record a lot of noise (possibly due to proximity to the airport) and the 400 MHz antenna to be quite ringy; the 200 MHz antenna seemed to provide a good compromise. We were able to collect data along the first 69 m of the profile line: we could not

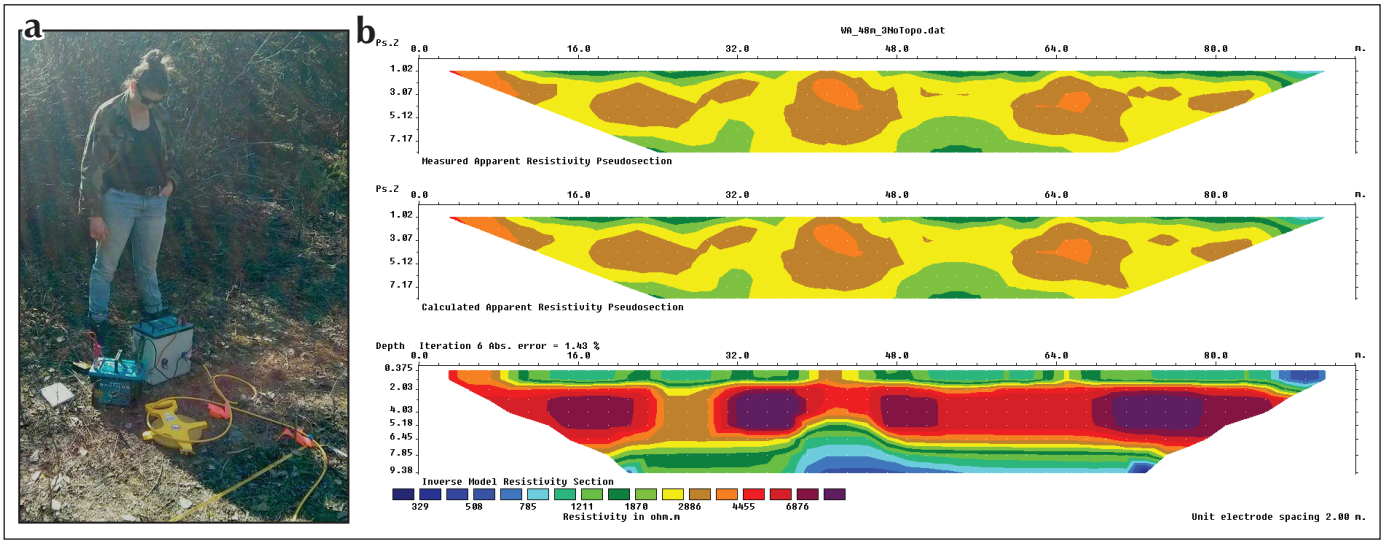

Figure 2. *Equipment and results for ERT.* ***(a)*** *IRIS-Syscal switch 48 in the field.* ***(b)*** *Data and inversion results as output by res2Dinv software; from top to bottom it shows the measured pseudosection, the calculated data, and the best-fit model. We note a high-resistivity (red colour) layer.*

continue farther with the antenna because the vegetation became too dense. To determine the dielectric constant of the sub-surface material we buried a bottle at 50 cm depth; its reflection appeared at 15.0 ns two-way time, which corresponds to a dielectric constant of 9.2 which we used to convert the vertical time axis into a depth axis. The resulting profile is shown in Figure 5a.

SEISMIC REFRACTION ANALYSIS AND TOMOGRAPHY

This method uses the travel times of seismic P-waves refracted off interfaces in the ground to visualize the subsurface structures. In our seismic survey, a hammer and strike plate (Fig. 4a) were used to induce a single source placed every 10 m from 0 to 90 m, plus one at 96 m, and vertical 4.5 Hz geophones were planted into the ground spaced 2 m apart. A Geometrics Geode 24-channel seismograph recorded the seismic waves arriving at each geophone. The first arrivals were picked and initially analysed assuming flat horizontal interfaces (Reynolds, 2011) as shown in Figure 3b. The travel times were then fed into the MATLAB tomography inversion code of St. Clair (2015) to model the velocity structure of the subsurface, including lateral variations. The code iterates between ray tracing and matching calculated travel times to the observed ones until a reasonable fit is found. In contrast to the refraction analysis, tomography creates a smooth model and does not reproduce sharp boundaries.

RESULTS

ELECTRICAL RESISTIVITY TOMOGRAPHY

The results of the ERT survey (Fig. 2b, bottom) show three distinct layers within a maximum penetration depth of 10 m. The top layer yields low resistivity values ranging from 1000 to 2000 Ωm and extends from the surface to 2 m depth. From 2 to 8 m a high resistivity layer is present with resistivity around 4000 Ωm. This is underlain by a third layer with resistivity below 2000 Ωm. The ERT result in Figure 5a includes a 2000 Ωm contour line to separate these three layers. We note that our ERT results closely resemble those obtained by Laxton and Coates (2015).

RADAR SECTION

The 200 MHz radargram section with depth instead of a two-way time is shown in Figure 5b. The profile displays a shallow sub-horizontal reflection in the top metre. Dipping undulating reflections are visible to 6 m depth, where a distinct horizontal reflector is present throughout. We note that the two-way-time was converted to depth using the dielectric constant we determined for the top layer; this constant is likely different for the layers below. If, for example, the dielectric constant for the middle layer is 4 instead of 9.2, then the bottom reflector would be found at a depth of 9 m instead of 6 m.

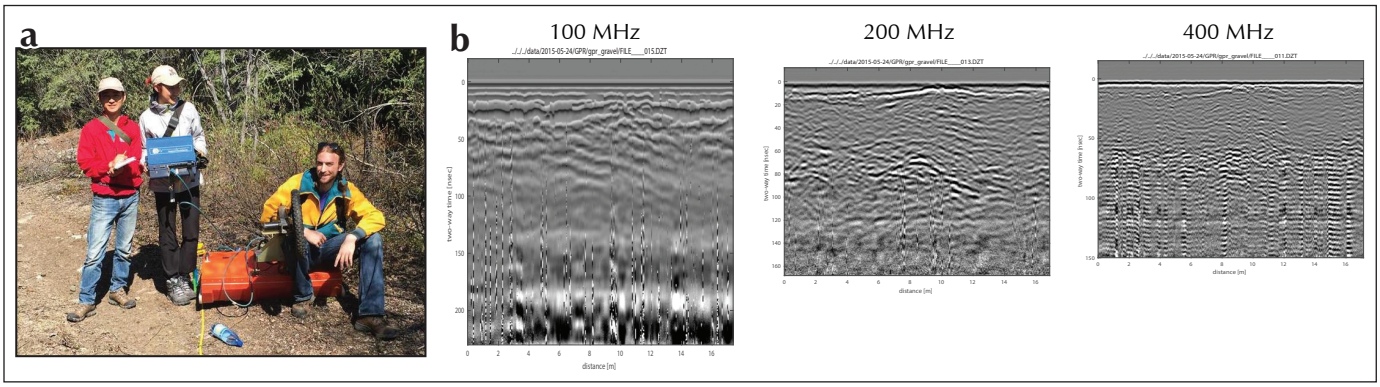

Figure 3. *GPR method.* ***(a)*** *Students presenting 100 MHz antenna, survey wheel, and console.* ***(b)*** *Testing of different antenne along the same short transect.*

SEISMIC REFRACTION ANALYSIS AND P-WAVE TOMOGRAPHY

A sample seismogram section in Figure 4b shows clear changes in slope of first arrivals at 20 m and 36 m which we can explain by a model with three horizontal layers: a 2.6 m thick layer with seismic velocity of 350 m/s, underlain by a 7.2 m thick layer with 670 m/s, and a bottom layer propagating seismic P-waves at 1780 m/s. We determined similar values for a reverse shot taken at 60 m distance. Deviations of observed travel times from the straight lines may be caused by topography on the boundary or lateral velocity variations; both can be imaged by seismic tomography. We picked 528 first arrivals (Fig. 4c) and the resulting seismic tomography image, which reproduce the root-mean square misfit of all travel times to within 1.3 ms, confirms this layered subsurface. Velocities below 500 m/s dominate the top 2 m, while at depth 2 to 10 m velocities range between 500 and 1300 m/s. From 8 to 15 m, layers with velocities below 2000 m/s are present. Beneath this depth, and to 25 m, the velocity increases to approximately 4500 m/s.

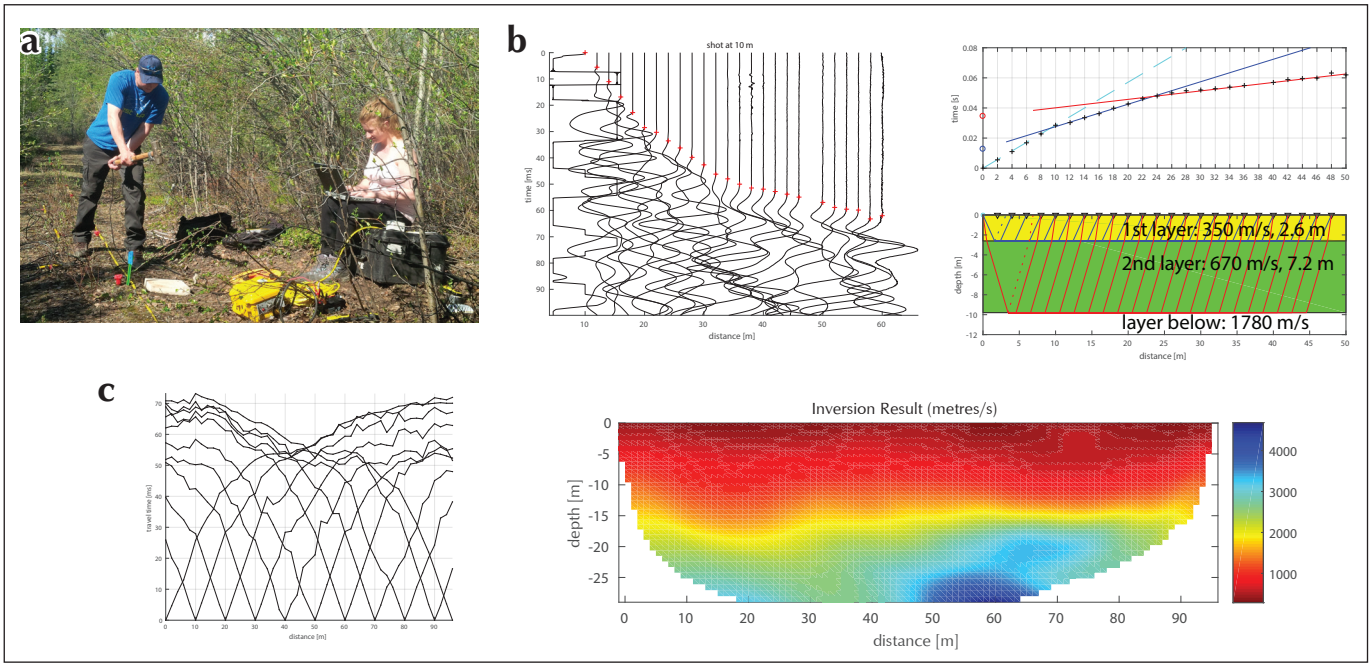

Figure 4. *Seismic equipment and results.* ***(a)*** *Energy originating when the sledgehammer hits strikeplate is picked up by red geophones connected to the yellow Geometrics Geode and saved onto the field laptop.* ***(b)*** *Sample shot - vertical traces show ground movement recorded at each geophone, and red plusses mark the first arrival - and analysis of this single shot reproducing a three-layer subsurface with horizontal and sharp interfaces.* ***(c)*** *528 travel times used for inversion and resulting smooth subsurface P-wave velocity model.*

DISCUSSION

We now compare and contrast the similarities and differences between the results obtained with the three geophysical methods (Fig. 5). They all display similar subsurface structures containing three distinct layers, though boundaries are not mapped at the same depths.

For the top 2 m our ERT results (Fig. 5a) show a low resistivity of 1000 to 2000 Ωm which may correspond to the soil and moist sandy gravel. In the radargram (Fig. 5b) a sub-horizontal reflection can be seen at depth between 0 and 1 m. These weaker reflections of the radio waves are interpreted as soft, unconsolidated material. Seismic results show a layer with a velocity of 350 m/s to 2.6 m depth. These velocity values usually correspond to a loosely compacted layer such as soil or sand.

Between 2 to 8 m, the ERT shows a value around 4000 Ωm while seismic velocities change from 400 to 1500 m/s. These velocities are within the range for gravel (Lucius, 2007; Reynolds, 2011). The dipping undulating reflections in the radargram correspond to a depth around 1 to 6 m and we interpret them as being caused by sedimentary structures within the gravel. A distinct horizontal reflector present at 6 m indicates a change in the dielectric constant; it may represent the boundary between the gravel layer and underlying till. This horizontal reflector is also the deepest penetration depth GPR can provide at our study site.

At below 8 to 10 m, a layer with low resistivity (~2500 Ωm) is present in the ERT results. This lower resistivity value may indicate a moist layer, or the underlying basalt bedrock with groundwater in fractures. The seismic refraction study finds a layer with 1780 m/s at that depth which would speak more for a compacted till layer (Reynolds, 2011). Seismic tomography provides us the deepest penetration and shows high velocities from

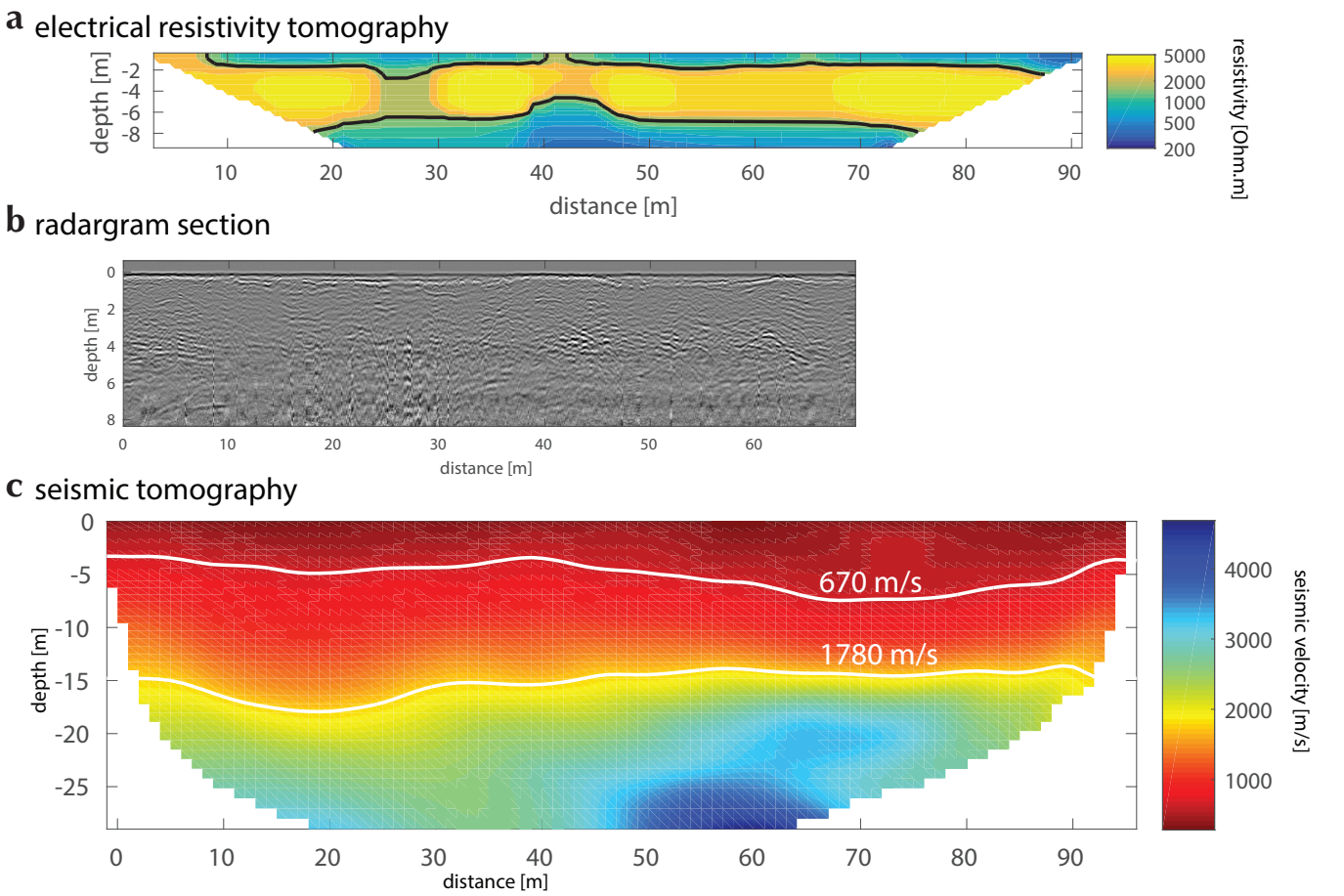

Figure 5. *Comparison of the three methods used in this study.* ***(a)*** *ERT results with 2000 Ωm contour to highlight resistive layer.* ***(b)*** *200 MHz radargram shows two continuous reflections, one near the surface and one at 6 m.* ***(c)*** *Seismic tomography result with two velocities from single shot analysis marked.*

2000 to 4500 m/s to a depth of ~30 m. The highest velocity obtained by the seismic tomography survey would likely point to fractured basaltic bedrock.

All three methods produced similar, albeit not the same, results; however, ERT was the easiest to set up even in thick vegetation and to model due to the fast inversion processing time. Simple analysis of seismic first arrivals produced quick results, while seismic tomography required filtering and significant data processing to produce a model comparable to ERT. GPR data also required filtering in order to show the main features, but did not provide the depth penetration of the other two methods, required determining (or assuming) the dielectric constant of the material to convert the two-way times to depth, and an antenna cannot be pulled along thickly vegetated profiles.

Whitehorse is situated in the Yukon Southern Lakes Ecoregion which is part of the sporadic discontinuous permafrost zone (Yukon Ecoregions Working Group, 2004; Heginbottom *et al.*, 1995). We were informed that ground ice was encountered at 50 cm depth two weeks prior to our survey (R. Gibson, *pers. comm.*). The ice encountered at the depth of 50 cm is probably ground ice caused by freezing processes during winter. Laxton and Coates (2015) mention that the presence of permafrost complicates the interpretation of resistivity measurements for gravel, as high resistivities of permafrost in fine-grained sediment can be similar to that of gravel. The presence of permafrost causes a change in resistivity values over several orders of magnitude. However, surveys undertaken by Laxton and Coates (2015) at the McLean Lake site, located ~2 km away from our survey site, show no presence of permafrost above 20 m. In our survey, resistivity values remain below 10 000 Ohm/m which would be a lower bound for permafrost (Laxton and Coates, 2015). The absence of permafrost is also supported by the absence of chaotic signals in radargrams indicative of massive ice or very ice-rich conditions (Laxton and Coates, 2011). Our seismic results also confirm the absence of permafrost. P-wave velocity increases predominantly as a result of ice pressure and to a lesser extent the higher velocity of ice compared to water in pores (Draebing and Krautblatter., 2012). The P-wave velocity of permafrost is about 3500 m/s (Sharma, 1997) which is above the velocity values we find in the top 15 m. Thus, we conclude that our survey did not encounter permafrost within the gravel layer.

CONCLUSION

Understanding the thickness and extent of this gravel deposit near Whitehorse is important for evaluating its potential as an aggregate quarry. The different geophysical methods we employed image contrasts in different physical properties (ground resistivity, dielectric constant, seismic velocity) which we need to interpret in terms of likely subsurface material. Therefore results are not the same; nevertheless we find a coherent trend in our results for the three methods. We interpret the top 2 m as soil and sandy gravel and the middle layer at depths of 2 to 8 m as gravel. This layer is then underlain by glacial till and/or bedrock. Overall, ERT seems to provide the clearest results and was the easiest method in this survey because it does not require a lot of post-collection data processing. Seismic refraction allowed for deepest imaging, and initial analysis of first breaks from a single shot already images sharp velocity changes. GPR is most intuitive in the field, also offers good insights and is the fastest to collect in the field, but conversion of the recorded two-way time to depth is not straight-forward and the energy does not penetrate as deep as for the other methods.

The presence of permafrost could affect our data. However, results from all three geophysical techniques indicate that permafrost is not present at our survey site to at least 15 m depth. Recommendations for future surveys include: conducting the survey during late summer to avoid the issue of seasonal ground ice and to run the survey on an exposed cut bank or drill along the survey transect to confirm the geophysical results.

ACKNOWLEDGEMENTS

We are grateful to University of Toronto Faculty of Arts and Science Research Excursion Program which funded this research trip. We would like to thank the other team members: Camille Hérbert, Yepin Zhang, Roberta Sears, William McNeice, Jamyang Jiangyangdingzhen, Norbert Kapa and Konstantinos Sacha Papadimitrios for their hard work in collecting data and great accompaniment during the trip. Staff at the Yukon Geological Survey provided logistical help to the UofT team, and Riley Gibson from All-In Exploration Solution Inc. offered guidance and information at the survey site. Thoughtful reviews by Ahmed Lachhab and Andrew Frederiksen helped improve the original manuscript.

REFERENCES

Bond, J., 2004. Late Wisconsinan McConnell glaciation of the Whitehorse map area (105D), Yukon. *In:* Yukon Exploration and Geology 2003, D.S. Emond and L.L. Lewis (eds.), Yukon Geological Survey, p. 73-88.

Draebing, D. and Krautblatter, M., 2012. P-wave velocity changes in freezing hard low-porosity rocks: a laboratory-based time-average model. The Cryosphere, vol. 6, p. 1163-1174.

Geotomo, 2009. Rapid 2-d resistivity and IP inversion using the least-squares method. Geotomo Software, Malaysia, 148 p.

Heginbottom, J.A., Dubreuil, M.A. and Harker, P.A., 1995. Canada – Permafrost, *In:* National Atlas of Canada, 5th Edition, National Atlas Information Service, Natural Resources Canada, MCR 4177.

Laxton, S., and Coates, J., 2015, Geophysical and borehole investigation of aggregate resources in the Whitehorse area, Yukon. Yukon Geological Survey, Open File 2015-1. Department of Energy, Mines and Resources, Government of Yukon.

Laxton, S., and Coates, J., 2011. Geophysical and borehole investigations of permafrost conditions associated with compromised infrastructure in Dawson and Ross River, Yukon. *In:* Yukon Exploration and Geology 2010, K.E. MacFarlane, L.H. Weston and C. Relf (eds.), Yukon Geological Survey, p. 135-148.

Loke, M.H., 2016. Tutorial: 2-D and 3-D electrical imaging surveys, 192 p., <http://www.geotomosoft.com/downloads.php> [accessed 28 November 2016].

Lucius, J.E., Abraham, J.D. and Burton, B.L., 2008. Resistivity profiling for mapping gravel layers that may control contaminant migration at the Amargosa Desert Research Site, Nevada. U.S. Geological Survey Scientific Investigations, Report 2008–5091, 30 p.

Lucius, J.E., Langer, W.H. and Ellefsen, K.J., 2007. An introduction to using surface geophysics to characterize sand and gravel deposits. U.S. Geological Survey Circular 1310, 33 p., <http://pubs.usgs.gov/circ/c1310/> [accessed 12 March 2016].

Reynolds, J.M., 2011. An introduction to applied and environmental geophysics, 2nd edition. John Wiley & Sons, West Sussex, England, 710 p.

Sharma, P.V., 1997. Environmental and engineering geophysics. Cambridge University Press, United Kingdom.

St. Clair, J., 2015. Geophysical investigations of underplating at the Middle American Trench, weathering in the critical zone, and snow water equivalent in seasonal snow. PhD thesis, University of Wyoming, USA, 163 p.

Yukon Ecoregions Working Group, 2004. Yukon Southern Lakes. *In:* Ecoregions of Yukon Territory: Biophysical properties of Yukon landscapes, C.A.S. Smith, J.C. Meikle and C.F. Roots (eds.), Agriculture and Agri-food Canada, PARC Technical Bulletin no. 04-01, Summerland, BC, p. 207-218.